Electronic Supplementary Material (ESI) for Physical Chemistry Chemical Physics.

Simultaneous Detection of Electronic Structure Changes from Two Elements of a Bifunctional Catalyst Using Wavelength-Dispersive X-ray Emission Spectroscopy and *in situ* Electrochemistry

Sheraz Gul[a,f], Jia Wei Desmond Ng[b], Roberto Alonso-Mori[c], Jan Kern[a,c], Dimosthenis Sokaras[c], Eitan Anzenberg[d], Benedikt Lassalle-Kaiser[a,#], Yelena Gorlin[b,%], Tsu-Chien Weng[c], Petrus Zwart[e], Jin Z. Zhang[f], Uwe Bergmann[c], Vittal K. Yachandra[a], Thomas F. Jaramillo[b,d,*] and Junko Yano[a,d,*]

[a]*Physical Biosciences Division, Lawrence Berkeley National Laboratory, Berkeley, CA 94720, USA.*
[b]*Department of Chemical Engineering, Stanford University, Stanford, CA 94305, USA.*
[c]*SLAC National Accelerator Laboratory, 2575 Sand Hill Rd., Menlo Park, CA 94025, USA.*
[d]*Joint Center for Artificial Photosynthesis, Lawrence Berkeley National Laboratory, Berkeley, CA 94720, USA.*
[e]*Advanced Light Source, Lawrence Berkeley National Laboratory, Berkeley, CA 94720, USA*
[f]*Department of Chemistry, University of California at Santa Cruz, Santa Cruz, CA 95060, USA.*
[#]*Present address: Synchrotron SOLEIL, L'Orme des Merisiers, Saint-Aubin, 91191 Gif-sur-Yvette, France.*
[%]*Present address: Technical University of Munich, Lichtenbergstrasse 4, 85748 Garching, Germany.*
[*]*Corresponding authors: jaramillo@stanford.edu, jyano@lbl.gov*

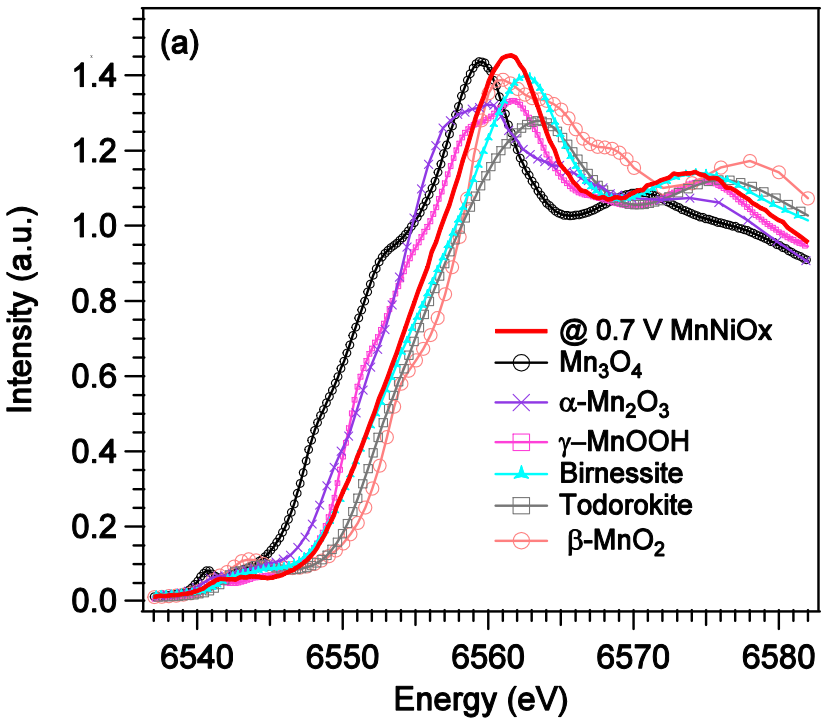

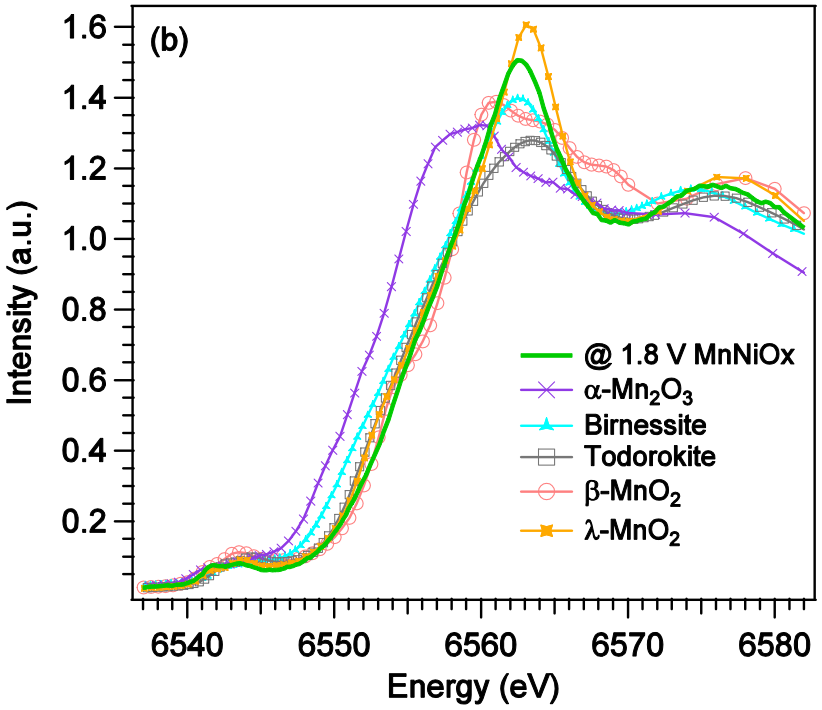

Fig. S1 (a) Mn *K*-edge spectrum of $MnNiO_x$ film poised at 0.7 V compared with Mn_3O_4, α-Mn_2O_3, γ-MnOOH, Mg^{2+}-birnessite, Todorokite and β-MnO_2. **(b)** $MnNiO_x$ sample held at 1.8 V overlaid with α-Mn_2O_3, Mg^{2+}-birnessite, Todorokite, β-MnO_2 and λ-MnO_2.

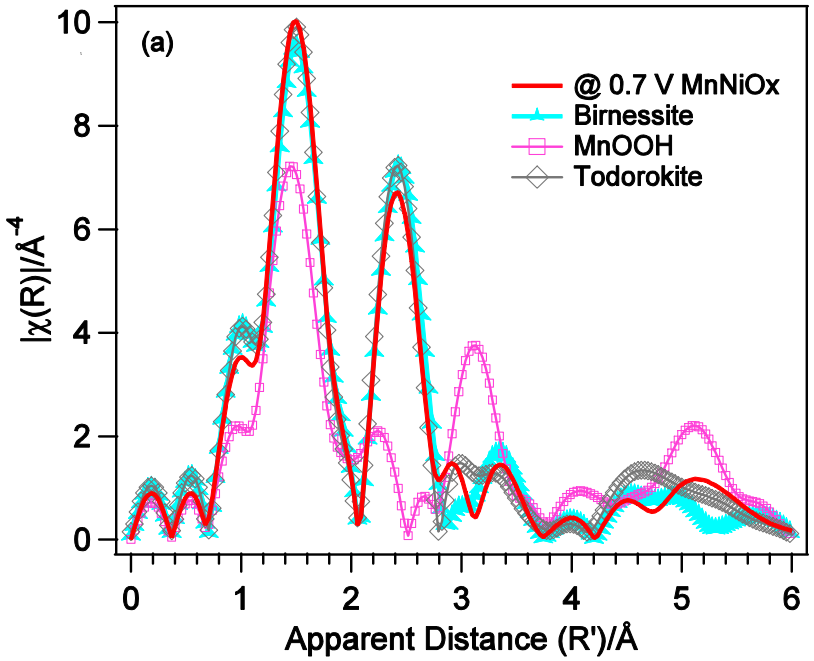

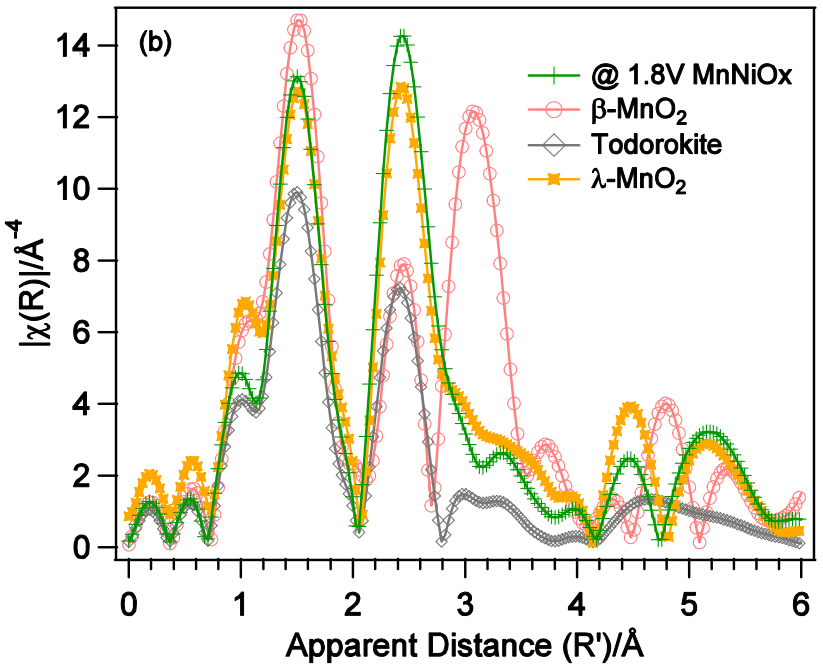

Fig. S2 (a) EXAFS spectra of ORR phase overlaid with Mg^{2+}-birnessite, Todorokite and MnOOH. The sample shows similarities with birnessite phase. **(b)** Comparison of the $MnNiO_x$ film poised at 1.8V with β-MnO_2, λ-MnO_2 and Todorokite.

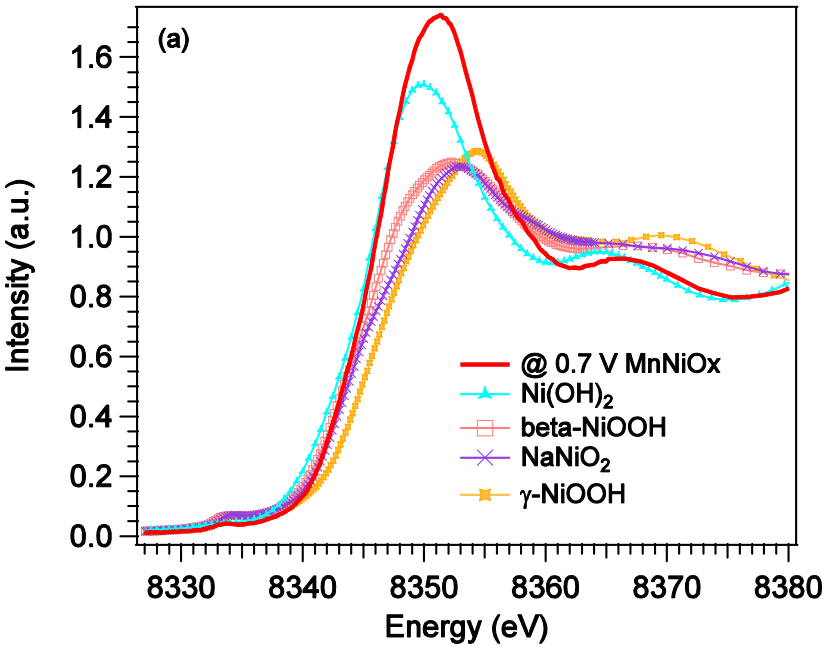

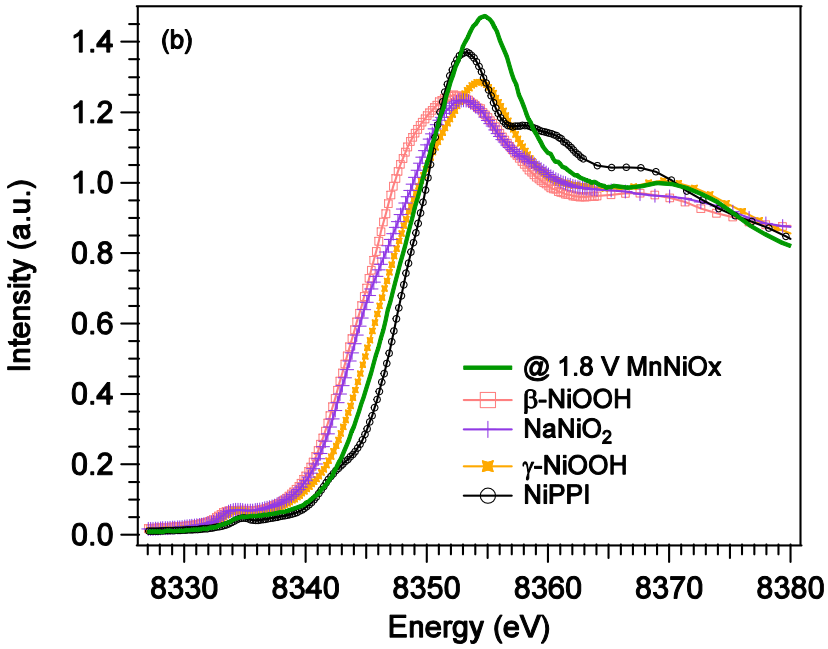

Fig. S3 (a) Ni *K*-edge spectrum of $MnNiO_x$ sample poised at 0.7 V overlaid with those of $Ni(OH)_2$, β-NiOOH, $NaNiO_2$ and γ-NiOOH. **(b)** $MnNiO_x$ sample under OER conditions compared with β-NiOOH, $NaNiO_2$, γ-NiOOH and NiPPI.

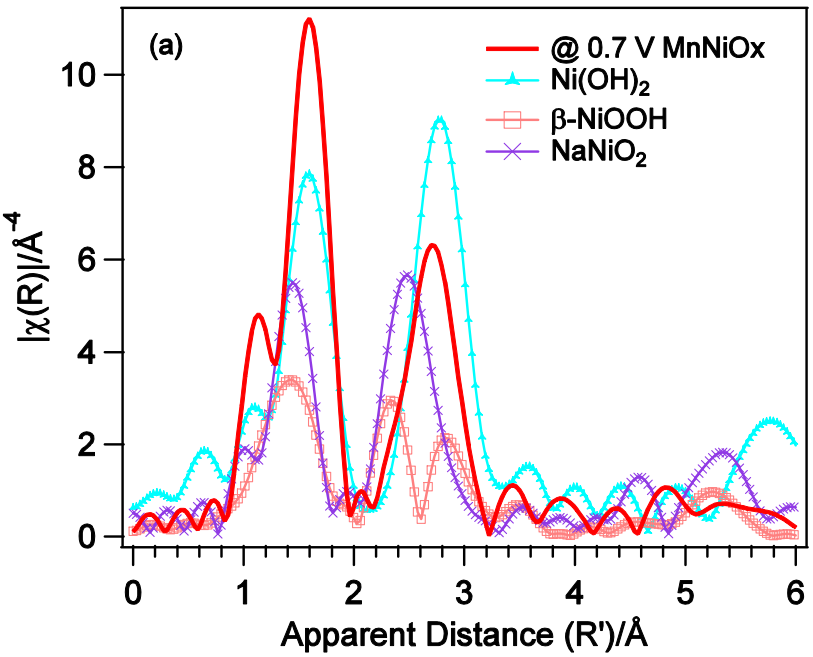

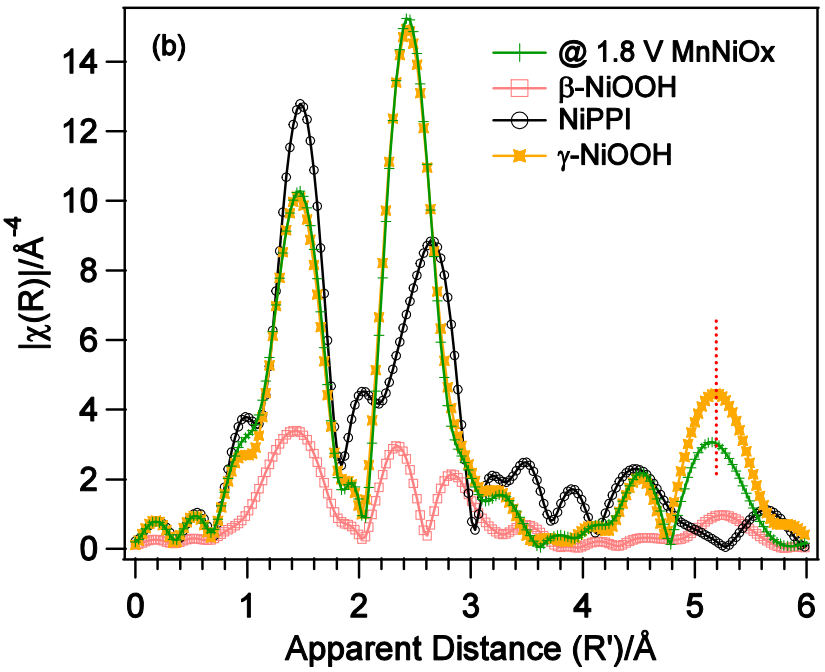

Fig. S4 (a) Fourier transformed EXAFS spectrum of $MnNiO_x$ sample poised at 0.7 V overlaid with $Ni(OH)_2$, $NaNiO_2$ and β-NiOOH. **(b)** Comparison of OER phase with β-NiOOH, γ-NiOOH, and NiPPI.

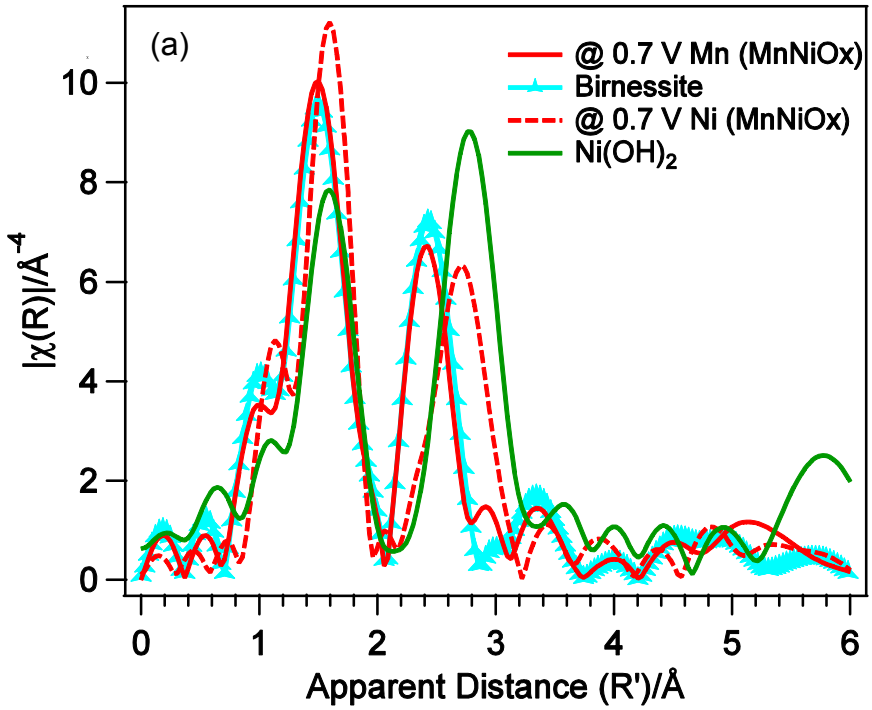

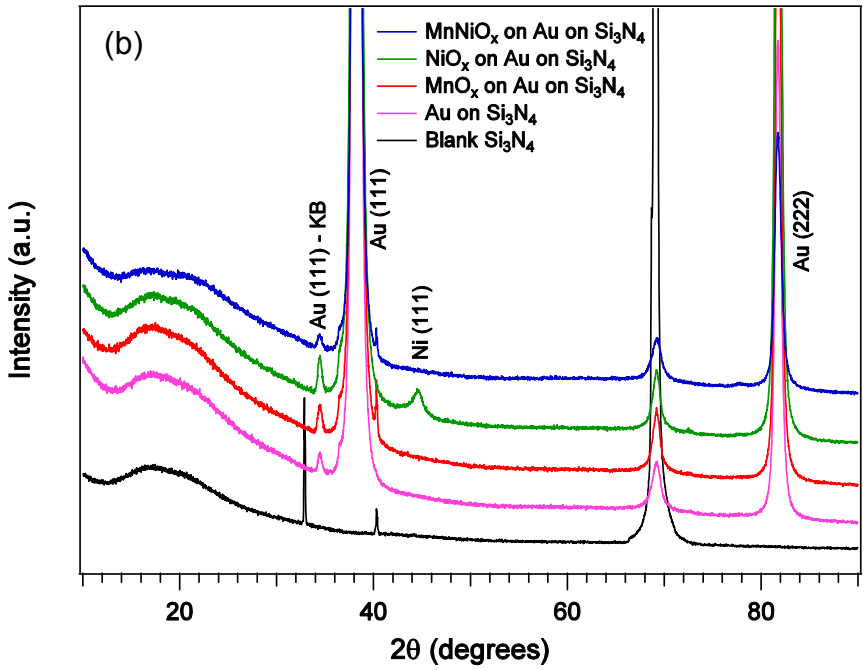
(b)
MnNiOx on Au on Si3N4
NiOx on Au on Si3N4
MnOx on Au on Si3N4
Au on Si3N4
Blank Si3N4
Au (111) - KB
Au (111)
Ni (111)
Au (222)
Intensity (a.u.)
20
40
60
80
2θ (degrees)

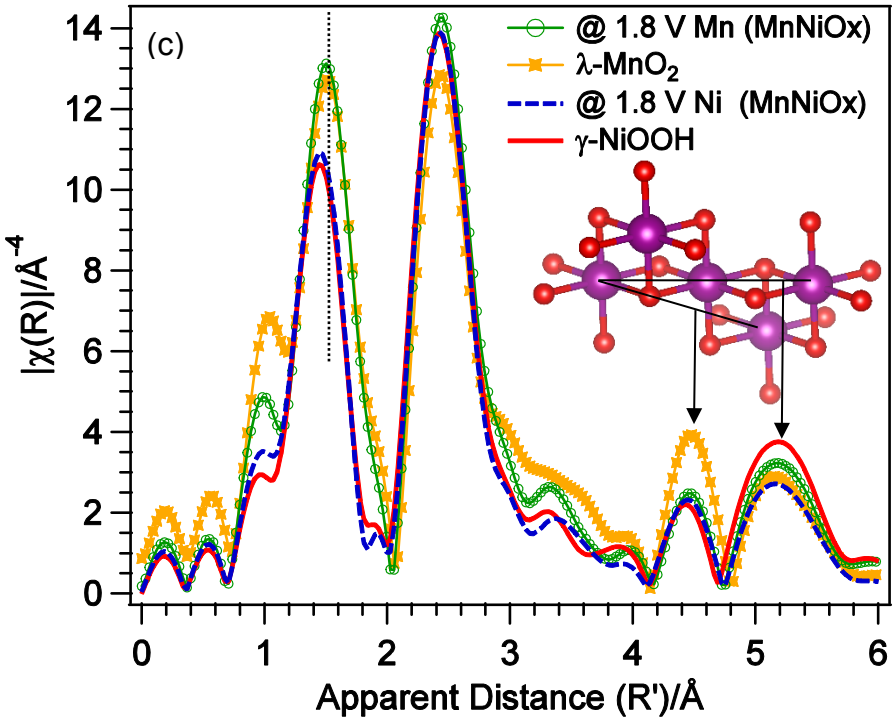
(c)
@ 1.8 V Mn (MnNiOx)
λ-MnO2
@ 1.8 V Ni (MnNiOx)
γ-NiOOH
|χ(R)|/Å-4
0
2
4
6
8
10
12
14
0
1
2
3
4
5
6
Apparent Distance (R')/Å

Fig. S5 (a) EXAFS spectra of $MnNiO_x$ at Mn and Ni *K*-edge under ORR conditions along with the corresponding model compounds **(b)** XRD diffractograms of (i) blank Si_3N_4, (ii) Au-coated Si_3N_4, (iii) MnO_x on Au-Si_3N_4, (iv) NiO_x on Au-Si_3N_4, and (v) $MnNiO_x$ on Au-Si_3N_4. **(c)** Mn and Ni *K*-edge Fourier transformed EXAFS spectra of $MnNiO_x$ sample under OER conditions overlaid with λ-MnO_2 and γ-NiOOH.

XAS of MnO_x

The MnO_x sample was prepared using a similar electrodeposition procedure as that of the $MnNiO_x$ sample except that Ni was absent from the deposition solution and only the Mn deposition potential (0.57 V vs. Ag/AgCl) was used, as described in the experimental section. *In situ* XAS measurements were performed on this MnO_x sample. The XANES spectra for the dry MnO_x sample is shown in **Fig. S6a** along with spectra measured *in situ* under ORR (0.7 V vs. RHE) and OER conditions (1.9 V vs. RHE), but at a higher potential as compared to $MnNiO_x$ (1.8 V vs. RHE) as no change was observed for the spectrum collected at 1.8 V (**Fig. S6b**). As the MnO_x sample is catalytically active for the OER at 1.8 V with no observable changes in the spectrum compared to that at 0.7 V, this suggests that a birnessite-like phase is responsible for the OER just as it was for the ORR. Increasing the potential to 1.9 V, however, resulted in a shift of the MnO_x spectrum to higher energy, indicating an increase in the oxidation state of Mn. This suggests that the presence of Ni in the $MnNiO_x$ sample had shifted the redox potential of Mn(III)/Mn(IV) to a lower value than for pure MnO_x . Mn *K*-edge XANES spectrum of the dry $MnNiO_x$ is also shown for comparison and the edge appears at lower energies as compared to that of dry MnO_x, in agreement with an overall higher oxidation state of Mn in the as prepared, dry MnO_x sample.

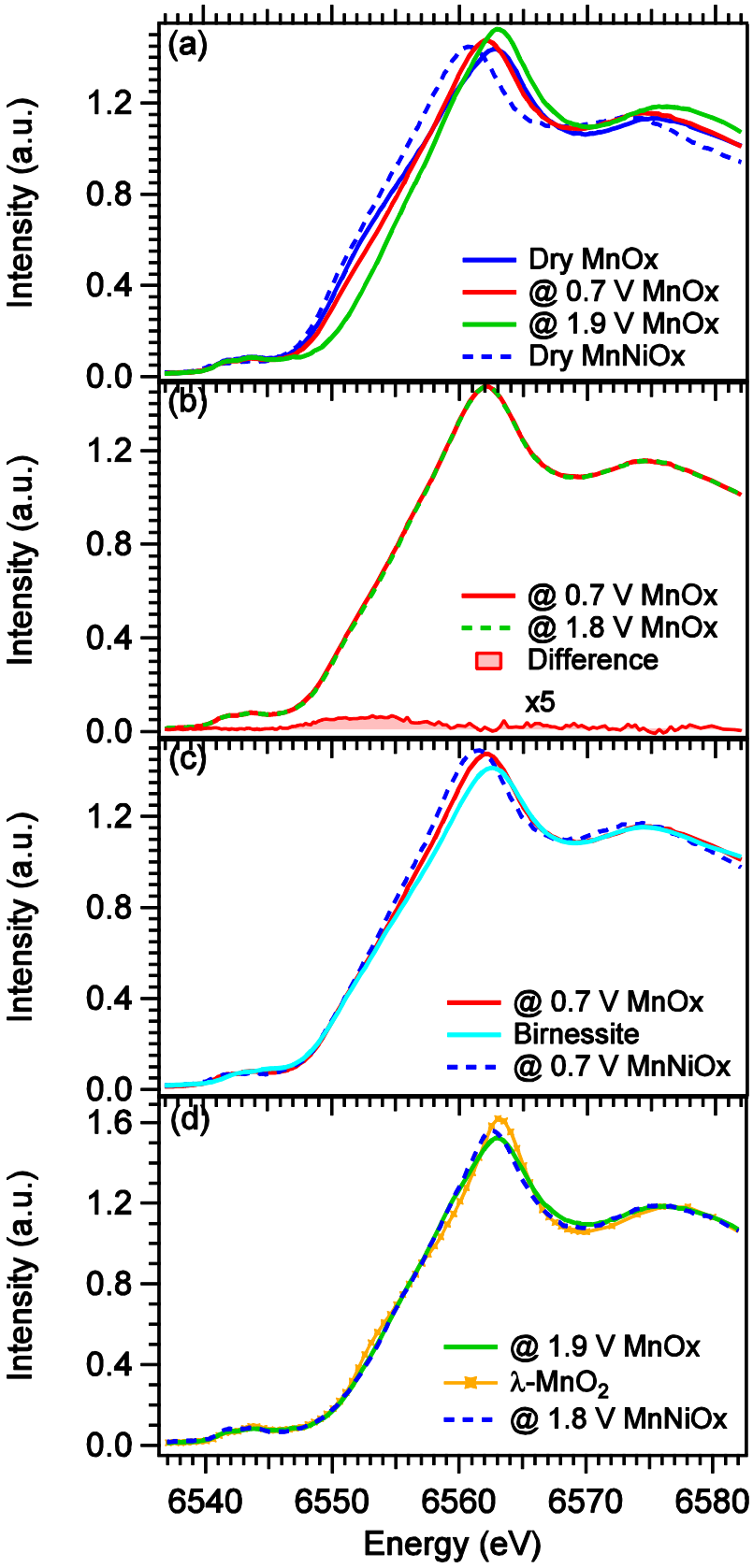
(a)
Intensity (a.u.)
1.2
0.8
0.4
0.0
Dry MnOx
@ 0.7 V MnOx
@ 1.9 V MnOx
Dry MnNiOx
(b)
Intensity (a.u.)
1.2
0.8
0.4
0.0
@ 0.7 V MnOx
@ 1.8 V MnOx
Difference
x5
(c)
Intensity (a.u.)
1.2
0.8
0.4
0.0
@ 0.7 V MnOx
Birnessite
@ 0.7 V MnNiOx
(d)
Intensity (a.u.)
1.6
1.2
0.8
0.4
0.0
@ 1.9 V MnOx
λ-MnO2
@ 1.8 V MnNiOx
6540
6550
6560
6570
6580
Energy (eV)

Fig. S6 (a) Mn *K*-edge XANES spectra of MnO_x when dry, under ORR (0.7 V) and OER (1.9 V) conditions. Mn XANES spectrum of dry $MnNiO_x$ is also shown for comparison. **(b)** XANES spectrum of MnO_x measured under ORR conditions (0.7 V) overlaid with the spectrum measured at 1.8 V. No significant change was observed when the potential was raised from 0.7 V to 1.8 V. The difference spectrum obtained by subtracting 1.8 V spectrum from that at 0.7 V is also shown to highlight the small change. **(c)** Spectrum of MnO_x ORR phase compared with Mg^{2+}-birnessite and Mn XAS spectrum of $MnNiO_x$ under ORR conditions. **(d)** Mn spectrum of MnO_x under OER conditions (1.9 V) overlaid with spectrum of λ-MnO_2 and $MnNiO_x$ under OER potential (1.8 V).

In **Fig. S6c**, the Mn *K*-edge spectrum of MnO_x at 0.7 V (ORR conditions) is compared with that of $MnNiO_x$ at the same potential as well as that of the birnessite standard. Much like the case with $MnNiO_x$, the MnO_x catalyst at ORR potentials shows similarities with birnessite, suggesting an oxidation state of Mn close to +3.6. **Fig. S6d** compares the XANES spectrum of MnO_x under OER conditions (1.9 V) with that of $MnNiO_x$ under similar OER conditions (1.8 V), in comparison with the λ-MnO_2 standard. Again, the spectra resemble that of λ-MnO_2, indicating a Mn oxidation state of +4. We note that the observed oxidation states exhibited by MnO_x under either ORR or OER potentials can depend greatly on the synthesis route, as reflected by the slight differences reported here versus those from a previous MnO_x study in which a different synthetic route involving a calcination step was employed.[1] Our ongoing work aims to elucidate how and why these differences occur.

The EXAFS spectra of MnO_x under ORR and OER conditions along with those of dry MnO_x and $MnNiO_x$ are shown in **Fig. S7a**. For MnO_x the peaks have higher amplitudes as compared to those of dry $MnNiO_x$, and reasonable amplitudes are observed for peaks between 4-6 Å that originate from the multiple scattering. This indicates a more long range order structure in MnO_x as compared to the mixed oxide. This is expected as $MnNiO_x$ was deposited layer by layer, alternating between Mn and Ni, which is prone to have some degree of disorder. Whereas EXAFS traces derived from dry MnO_x and under OER conditions have considerable amplitude between 5-6 apparent distance, the intensity is reduced under ORR conditions. This suggests that the ORR phase has a higher degree of structural disorder. However, the ORR phase of MnO_x has a more ordered lattice than

the ORR phase in $MnNiO_x$, as demonstrated by **Fig. S7b** where the EXAFS intensity for the former is higher. On the other hand, as revealed in **Fig. S7c**, the OER phase was found to be slightly more ordered in $MnNiO_x$ as compared to MnO_x. Attempts were also made to study the pure NiO_x phase, but XAS signal was dominated by metallic Ni and changes happening at the electrochemically active oxide surface were buried underneath. Long range order and presence of metallic Ni was also observed in XRD data (**Fig. S5b**).

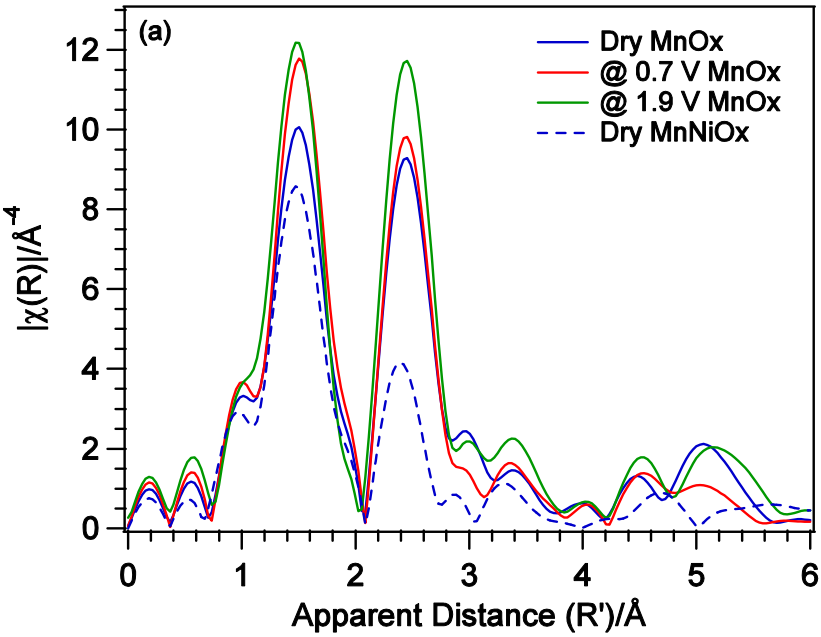

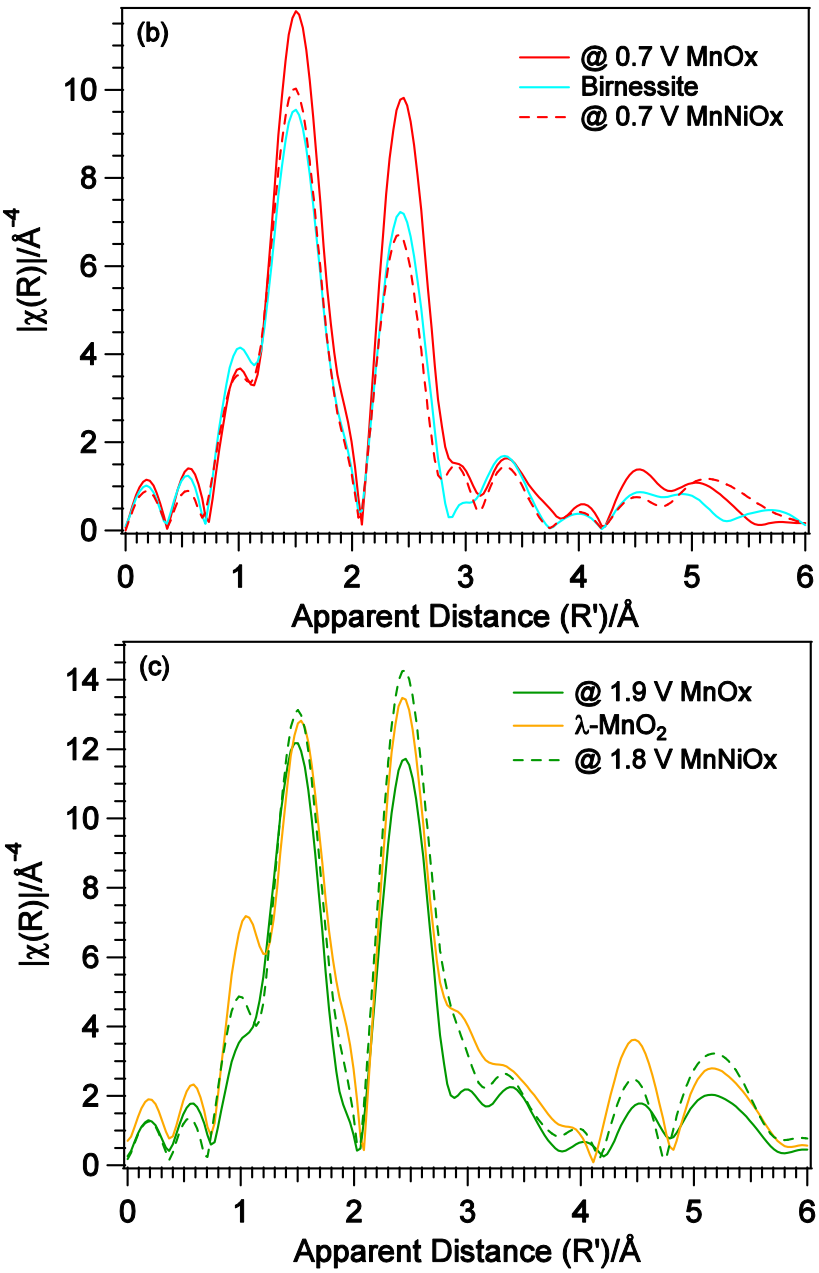

Fig. S7 (a) Mn *K*-edge EXAFS spectra of MnO_x under dry, ORR (0.7V) and OER (1.9 V) conditions. For comparison, EXAFS spectrum of dry $MnNiO_x$ is also shown. **(b)** EXAFS spectra of MnO_x ORR phase overlaid with Mg^{2+}-birnessite, ORR phase of $MnNiO_x$. The sample shows similarities with birnessite phase. **(c)** Comparison of the MnO_x electrocatalyst poised at 1.9 V with, λ-MnO_2 and Mn EXAFS spectrum of $MnNiO_x$ collected at 1.8 V.

Table S1: Atomic distances obtained from EXAFS curvefitting .

<ORR>

	$MnNiO_x$	$Ni(OH)_2$	birnessite	λ-MnO_2
Ni-O	2.06 (0.01)	2.06 (0.01)		
Mn-O	1.92 (0.01)		1.90 (0.01)	1.90 (0.02)
Ni-M	3.06 (0.01)	3.12 (0.01)		
Mn-M	2.88 (0.01)		2.88 (0.01)	2.86 (0.01)

<OER>

	$MnNiO_x$	γ-NiOOH	birnessite	λ-MnO_2
Ni-O	1.89 (0.01)	1.88 (0.01)		
Mn-O	1.90 (0.01)		1.90 (0.01)	1.90 (0.02)
Ni-M	2.83 (0.01)	2.82 (0.01)		
Mn-M	2.87 (0.01)		2.88 (0.01)	2.86 (0.01)

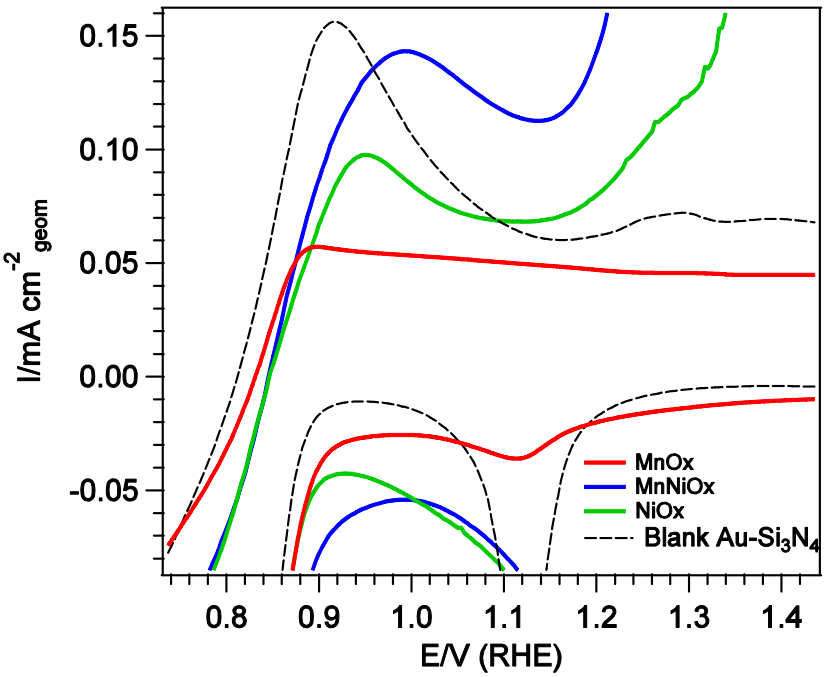

Fig. S8 Cyclic voltammogram also does not show any distinct oxidation peak in the case of MnO_x, as such a feature would likely be hidden underneath the capacitive behavior. The small reduction peak around 1.1 V corresponds to gold reduction.

References

1. Y. Gorlin, B. Lassalle-Kaiser, J. D. Benck, S. Gul, S. M. Webb, V. K. Yachandra, J. Yano and T. F. Jaramillo, *Journal of the American Chemical Society*, 2013, **135**, 8525-8534.